

Ambient ultrasonic-assisted synthesis, stepwise growth mechanisms, and photocatalytic activity of flower-like nanostructured ZnO and Ag/ZnO

Yingming Zhu · Dongsheng Liu · Youlei Lai · Ming Meng

Received: 19 December 2013 / Accepted: 27 January 2014 / Published online: 18 February 2014
© Springer Science+Business Media Dordrecht 2014

Abstract Flower-like nanostructured ZnO and Ag/ZnO catalysts were synthesized at ambient condition by a facile one-pot ultrasonic irradiation process. The ZnO morphology could be modified by both ultrasonic frequency and Ag amount. The acoustic cavitation effect dependent on ultrasonic frequency directly affects ZnO morphology. Doping of Ag not only promotes the transformation of zinc hydroxide to oxide, facilitating the formation of flower-like ZnO, but also enhances the photocatalytic degradation of Rhodamine B due to the promoted electron–hole segregation. The optimized ratio of Ag/Zn is 5 % (atomic ratio); more Ag can cover the surface of ZnO, decreasing the UV–vis light availability and mass transfer efficiency during reaction. The catalysts prepared at different ultrasonic frequencies show different UV–vis light absorbances and different UV–vis light availabilities. Among the catalysts of Ag/ZnO with 5 % Ag (ZA5-*x*), ZA5-100 prepared using 100 kHz ultrasonic frequency possesses the highest UV–vis light absorbance and best photocatalytic activity. Potential mechanisms for flower-like ZnO growth and Rhodamine B photodegradation are proposed.

Keywords Nano-materials · Photocatalysis · Zinc oxide · Silver · Ultrasonic synthesis

Introduction

Zinc oxide (ZnO) with a direct wide band gap (3.37 eV) and a large exciton binding energy (60 meV) have been widely used as a very important II–VI semiconductor in our daily life (Klingshirn et al. 2010). It is well known that nanoscale materials have many different properties from bulk materials, such as small size effect, surface effect, quantum effect, and macroscopic quantum tunnel effect (Buzea et al. 2007), so the synthesis and properties investigation of nano-materials have become one important research hotspot in the last two decades. Nano ZnO has also attracted much attention owing to its promising applications in the fields of piezoelectricity (Wang et al. 2004), emitter (Zhao et al. 2006), detector (Look 2001), solar cells (Zhang et al. 2008a), amplifier (Yamamoto 2000), sensor (Roy and Basu 2002), and so on. Up to now, lots of methods have been developed for the preparation of nano ZnO, and various kinds of nanostructured ZnO materials have been successfully fabricated (Wang 2004). However, most of these methods often need rigorous conditions involving extreme reaction parameter, expensive equipments, and tedious operation steps. Therefore, the development of more facile preparation for nano ZnO materials is

Y. Zhu · D. Liu · Y. Lai · M. Meng (✉)
Collaborative Innovation Center for Chemical Science and Engineering (Tianjin), Tianjin Key Laboratory of Applied Catalysis Science & Engineering, School of Chemical Engineering and Technology, Tianjin University, Tianjin 300072, People's Republic of China
e-mail: mengm@tju.edu.cn

rather significant and highly expected, although there are so many challenges.

Ultrasonic wave, generally referring to the acoustic wave with frequency more than 20 kHz, is widely used in the laboratory and industry. It is well known that the ultrasonic can induce acoustic cavitation effect in the liquids, i.e., some small bubbles are formed, then grow, and then impulsively collapse under ultrasonic radiation (Suslick 1990). Because of the adiabatic compression of gas in these bubbles, a good deal of energy will be released during the implosive collapses process. As a result, many localized hotspots can be formed around these collapse bubbles. In the surrounding regions of these hotspots the pressure can reach as high as 20 MPa, and the transient temperature can reach nearly 5,000 K; however, the cooling rate can exceed 10^{10} K/s. The thickness of the hotspot region is about 200 nm from the bubbles interface, and the average lifetime of hotspots is only about 2 μ s. Due to the acoustic cavitation effect, ultrasonic can initiate some kinds of chemical reactions which cannot take place at ambient condition, such as the decomposition of H_2O to H^\cdot and OH^\cdot . This property of ultrasonic makes it highly applicable in the field of nano-materials synthesis (Bang and Suslick 2010). In recent years, lots of ZnO nanostructures have been successfully synthesized by many methods with ultrasonic assistance (Zheng et al. 2010; Zhou et al. 2006; Zhang et al. 2008b; Mishra et al. 2010; Uma et al. 2009). However, ultrasonic is mainly used for the pretreatment or posttreatment of solutions, suspensions, or solid precursors at required temperatures during nano-materials preparation. Up to now, only a few works have been focused on the synthesis of nano ZnO directly using ultrasonic irradiation at room temperature (Amir et al. 2013; Liu et al. 2012; Jung et al. 2008). However, as far as we know, the influence of ultrasonic frequency on the synthesis of flower-like nano ZnO is seldom reported. Actually, compared with conventional methods, such as co-precipitation, sol-gel, emulsion, hydrothermal synthesis, etc., the method of ambient independent ultrasonic irradiation possesses many advantages, e.g., the short reaction time, simplicity of operation, convenience of equipment, low energy consumption, and potential large-scale industrialization, and thus the exploration and employment of ambient independent ultrasonic irradiation for the synthesis of nano-materials including ZnO is of great significance.

With the rapid development of industry, water pollution becomes more and more serious. Traditional water treatments are mainly based on physical methods, such as adsorption, filter, and sedimentation, which usually need further treatment and may result in the secondary pollution. Photocatalytic degradation can overcome these shortcomings by directly removing various pollutants in wastewater with high efficiency (Bhatkhande et al. 2001). Generally, when the semiconductor is irradiated by the light with energy equal to or higher than its band gap, the electrons of the valence band (VB) can be excited to the conduction band (CB) and leave the holes in VB for charge balance. Some of these electrons and holes can migrate to the semiconductor surface and then be captured by oxygen and surface hydroxyl species, respectively, further forming the superoxide radical anion ($O_2^\cdot-$) and hydroxide free radical (OH^\cdot) which are highly active for pollutants degradation. However, the electrons and holes are inclined to recombine before reacting with pollutants. So, the high-segregation efficiencies of electrons and holes are rather important for good photocatalysts (McCullagh et al. 2011; Gerven et al. 2007). For nanosized ZnO, the mean free path of electrons is also in nanoscale, which makes the electrons and holes readily migrate to the surface for reactions, as a result, the nano ZnO materials often show much better photocatalytic activity than bulk ones (Murphy and Jana 2002; Liu et al. 2009). In addition, it has been found that the interaction between Ag and ZnO can effectively inhibit the electron-hole recombination due to the electron sink effect of Ag (Georgekutty et al. 2008; Zheng et al. 2007a; Zhang and Mu 2007; Lai et al. 2010). Therefore, the doping of Ag to ZnO is an effective way to improve its photocatalytic activity.

In present work, a series of flower-like ZnO and Ag/ZnO photocatalysts were successfully fabricated by a facile one-pot ultrasonic irradiation process at ambient condition. The synthesized materials are characterized by X-ray diffraction (XRD), field-emission scanning electron microscopy (FESEM), transmission electron microscopy (TEM), UV-vis diffuse reflectance spectroscopy (UV-vis DRS), Fourier transform infrared spectroscopy (FT-IR), and thermogravimetric analysis (TG). It is found that the ultrasonic frequency determines the energy released from the acoustic cavitation effect, which can be employed to adjust the morphology of nano ZnO materials; the doping of Ag^+

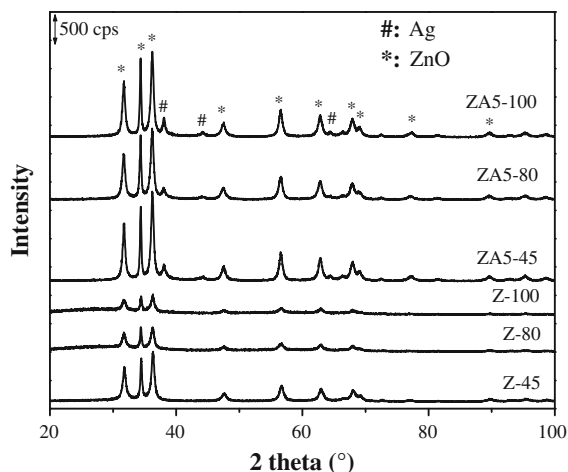


Fig. 1 XRD patterns of the catalysts ZA5-*x* and Z-*x*

promotes the transformation of zinc hydroxide to zinc oxide, facilitating the formation of nanostructured flower-like ZnO. Based upon multiple characterization results, the influences of both the ultrasonic frequency and the dosage of Ag^+ on the photocatalytic activity of ZnO for Rhodamine B degradation are carefully investigated; meanwhile, potential stepwise mechanisms for flower-like ZnO growth and for Rhodamine B photodegradation over as-synthesized ZnO and Ag/ZnO are proposed or discussed particularly.

Results and discussion

Characterization results

Figure 1 shows the XRD patterns of as-synthesized catalysts Z-*x* and that doped with 5 % Ag (ZA5-*x*). It can be seen that for the catalysts Z-*x* only wurtzite-structured hexagonal ZnO (JCPDS 65-3411) is detected, while for ZA5-*x* face-centered-cubic (FCC) metallic Ag (JCPDS 65-2871) can also be identified except for hexagonal ZnO phase. No obvious shift for the diffraction peaks of ZnO in the XRD patterns of ZA5-*x* is observed, indicating that no solid solution between Ag and ZnO is formed (Zheng et al. 2007a). These results demonstrate that ZnO or Ag/ZnO has been successfully synthesized through the facile independent ultrasonic irradiation method. Comparing the XRD patterns of ZA5-*x* with those of Z-*x*, it is easily found that all the diffraction peaks of ZA5-*x* are

much stronger and sharper than those of Z-*x*, suggesting that the doping of Ag into ZnO can facilitate the crystallization of ZnO. For the catalysts Z-*x*, with the increase of ultrasonic frequency the diffraction peaks gradually become weaker, implying the decrease of ZnO crystallization degree.

Figure 2 shows the SEM images of the catalysts Z-*x*. It is clearly seen that some flower-like structures are formed in both of Z-45 and Z-80 samples although their appearances are different. The diameter of the flower in Z-45 is about 2 μm , while it is nearly 5 μm in Z-80. Some irregular particles and blocks are also found on the surface of these flowers in Z-45 and Z-80 catalysts as shown in Fig. 2a–d. For Z-100, its morphology seems quite different from those of Z-45 and Z-80. As shown in Fig. 2e, no any flower-like structure in Z-100 can be found except the blocks. These blocks are formed by the aggregation of some irregular particles as seen in Fig. 2f. Therefore, it is concluded that low-ultrasonic frequency used in the preparation is more favorable to the formation of flower-like morphology of ZnO.

The SEM images of Ag-doped catalysts ZA5-45, ZA5-80, and ZA5-100 are shown in Fig. 3. It is found that the morphology of ZnO changes a lot after Ag is doped. From the SEM images of ZA5-45, as shown in Fig. 3a, b, it can be seen that some flower-like structures with the diameter of several hundred nanometers can be distinguished, which is quite different from that of Z-45 in Fig. 2a, b. These flowers adhere to each other irregularly, leading to the formation of some blocks. The morphologies of ZA5-80 and ZA5-100 are similar to each other, showing uniform and well-defined flower-like structures as shown in Fig. 3c–f, but they are also different from those for Z-80 and Z-100 in Fig. 2c–f. In addition, it is worth noting that there are also many small spheres which are randomly scattering on the surface of all ZA5-*x* samples as seen in Fig. 3. By comparison, it is summarized that the doping of Ag into ZnO can greatly influence its morphology under ultrasonic irradiation, especially at higher ultrasonic frequency, such as 80 and 100 kHz.

Figure 4a, b are the TEM images of ZA5-100 with low and high magnification, respectively. It is observed that during TEM tests, the flower-like structures in ZA5-100 can be very well maintained and the small spheres are still strongly attached on the surface. The local EDS analysis on the designated area

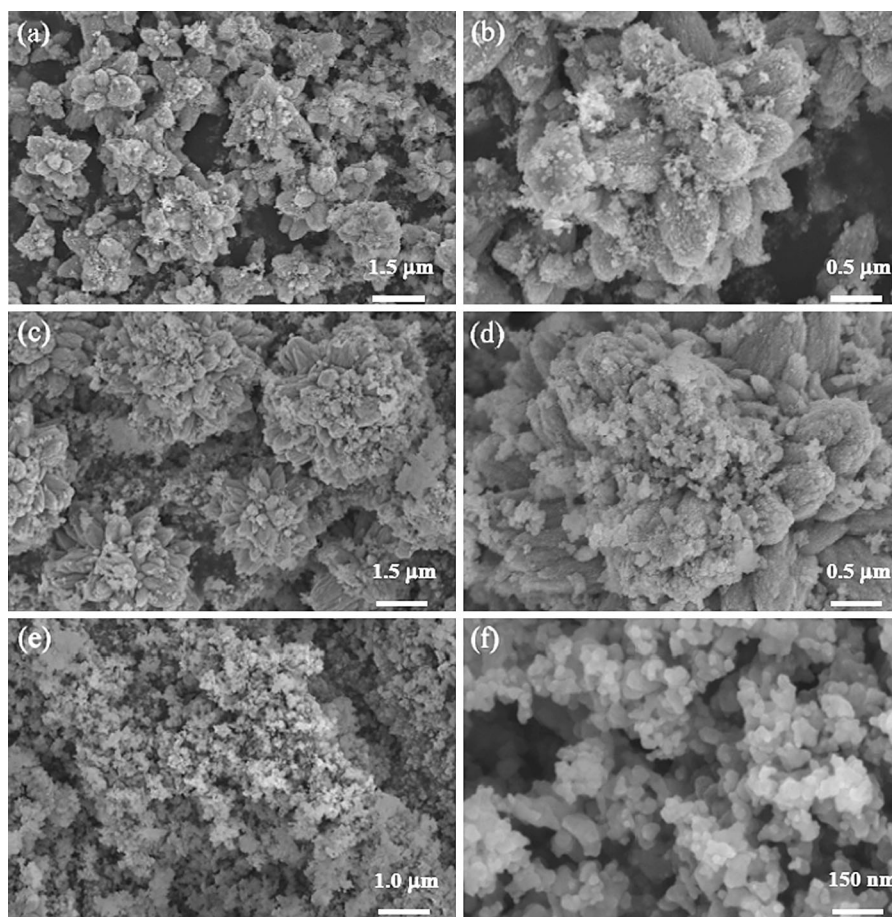


Fig. 2 SEM images of Z-*x* catalysts: **a, b** for Z-45; **c, d** for Z-80; **e, f** for Z-100

in Fig. 4b confirms that this sample is only composed of Ag, Zn, and O elements (C and Cu come from the copper grid used for supporting sample during TEM measurement) as seen in Fig. 4c, indicating that Ag has been successfully doped into the ZnO sample via a facile one-pot independent ultrasonic irradiation.

Figure 5 shows the UV-vis spectra of Z-*x* and ZA5-*x*. The characteristic absorption edge of ZnO can be distinguished in both Z-*x* and ZA5-*x* as indicated in Fig. 5a, b, however, the UV-vis absorption performance is apparently changed as Ag is doped. From Fig. 5b, it can be clearly seen that there is also an absorption band near 490 nm for all the ZA5-*x* catalysts besides the absorption edge of ZnO, which can be assigned to the characteristic absorption of surface plasmon resonance (SPR) caused by nano metallic Ag (Zheng et al. 2007a). In addition, by comparing Fig. 5b with Fig. 5a, it can still be found that the UV-vis absorbance is greatly enhanced after Ag doping.

Among the catalysts of Z-*x*, Z-45 shows the highest absorbance with a value of 0.5 in the UV area. In the catalysts ZA5-*x*, ZA5-80 exhibits the lowest absorbance but the absorbance value is even near to 0.5 in the visual light area. The UV-vis results further confirm the successful formation of ZnO or Ag/ZnO by the facile independent ultrasonic irradiation, which show good UV-vis absorption performance.

Figure 6 shows the FT-IR spectra of ZA5-*x* and Z-*x*. The absorption band at 500 cm^{-1} is assigned to the characteristic absorption of ZnO (Zheng et al. 2007b), which can be distinguished in all the spectra for ZA5-*x* and Z-*x* samples. All the absorption bands of ZnO for Z-45 are much stronger than those for Z-80 and Z-100. These results are consistent with those of XRD, and further evidence that both the employment of low-ultrasonic frequency and the doping of Ag are favorable to the formation of ZnO crystal. However, in the catalysts ZA5-*x* and Z-*x* the presence of a small

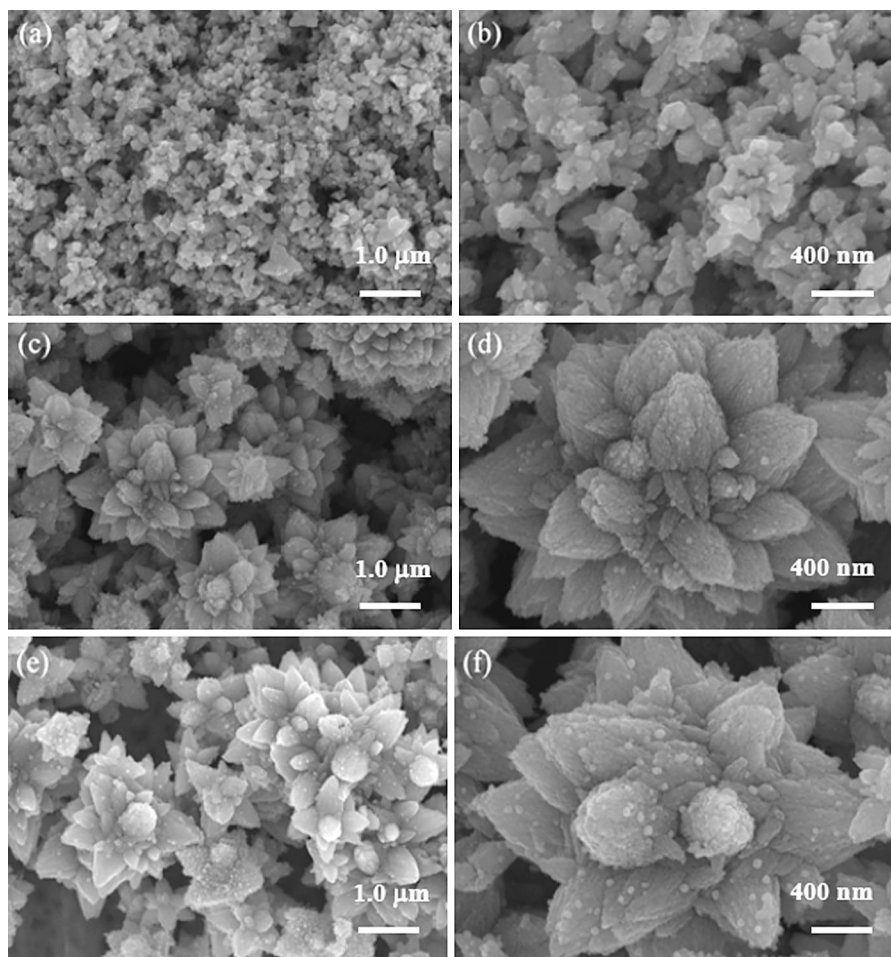


Fig. 3 SEM images of ZA5-*x* catalysts: **a, b** for ZA5-45; **c, d** for ZA5-80; **e, f** for ZA5-100

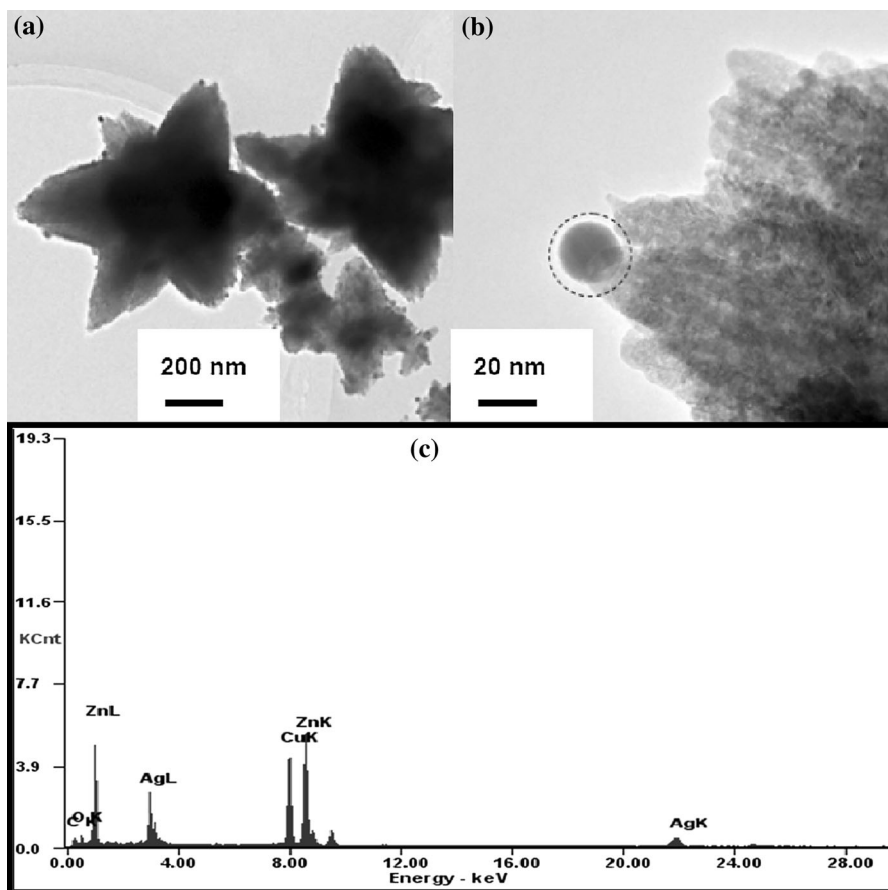
amount of hydroxides such as $\text{Zn}(\text{OH})_2$ and AgOH cannot be totally excluded, although the FT-IR spectra show no characteristic bands of them. To make clear of this point, the samples are characterized by TG technique, the results of which are shown in Fig. 7. It is seen that the weight loss of each catalyst is very low before 120 °C, and the main weight loss occurs between 120 and 350 °C. The weight loss before 120 °C can be assigned to the volatilization of surface adsorbed water, while the main weight loss between 120 and 350 °C is attributed to the thermal decomposition of hydroxide such as $\text{Zn}(\text{OH})_2$ and AgOH . The gradual weight loss after 350 °C corresponds to the gradual loss of surface hydroxyl groups in the form of water (Lai et al. 2011). To know the influence of ultrasonic frequency and Ag doping on the growth of ZnO, the total weight loss from room temperature to

800 °C of each catalyst is calculated and listed in Table 1. It can be seen that the weight loss increases with the elevation of ultrasonic frequency used in the preparation, and the weight loss of Z-*x* is much larger than that of the corresponding ZA5-*x* catalyst. That is to say, both the low-ultrasonic frequency and the doping of Ag can effectively decrease the contents of hydroxides, which is favorable to the formation of ZnO crystal and the increase of photocatalytic activity.

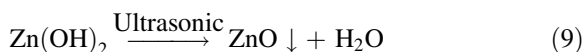
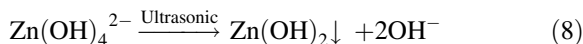
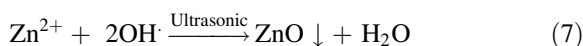
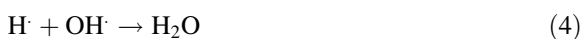
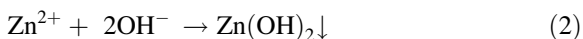
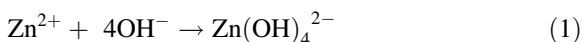
Growth mechanism

In the alkali solution and at room temperature, the $\text{Zn}(\text{OH})_4^{2-}$ or $\text{Zn}(\text{OH})_2$ species are easily formed, as shown by Eqs. 1 and 2, but they cannot directly transform to ZnO. After the employment of ultrasonic irradiation during preparation, the situation will change

Fig. 4 **a** TEM image of ZA5-100 with low magnification; **b** TEM image of ZA5-100 with high magnification; **c** EDS analysis results corresponding to the *circle* area indicated in **(b)**



a lot. Due to the acoustic cavitation effect, the ultrasonic irradiation can initiate some kinds of chemical reactions which hardly take place at ambient condition, such as the decomposition of H_2O into H^\cdot and OH^\cdot radicals as shown in Eq. 3. Although most of these radicals will be immediately consumed through the reaction between themselves as indicated in Eqs. 4–6, some radicals can still be captured by zinc ions and then leading to the formation of ZnO as shown in Eq. 7. In addition, ultrasonic irradiation can also promote the transformation of $\text{Zn}(\text{OH})_4^{2-}$ to $\text{Zn}(\text{OH})_2$ and/or $\text{Zn}(\text{OH})_2$ to ZnO , further facilitating the formation of ZnO (Mazloumi et al. 2009), as presented in Eqs. 8 and 9.



The ultrasonic frequency can influence the acoustic cavitation effect and then affect the formation of ZnO . Scheme 1 shows the energy released during the bubble collapse process under ultrasonic irradiation with different frequencies. When low-ultrasonic frequency is used as shown in Scheme 1a, not many bubbles can be formed and they distribute evenly in the liquid. Under the continuous irradiation of ultrasonic, these bubbles grow and the gas in them will undergo the adiabatic compression, leading to the implosive collapse. Due to the low quantity and the even distribution of bubbles in the solution, each bubble can be fully surrounded by liquid. In this condition, the energy released from the implosive collapses process

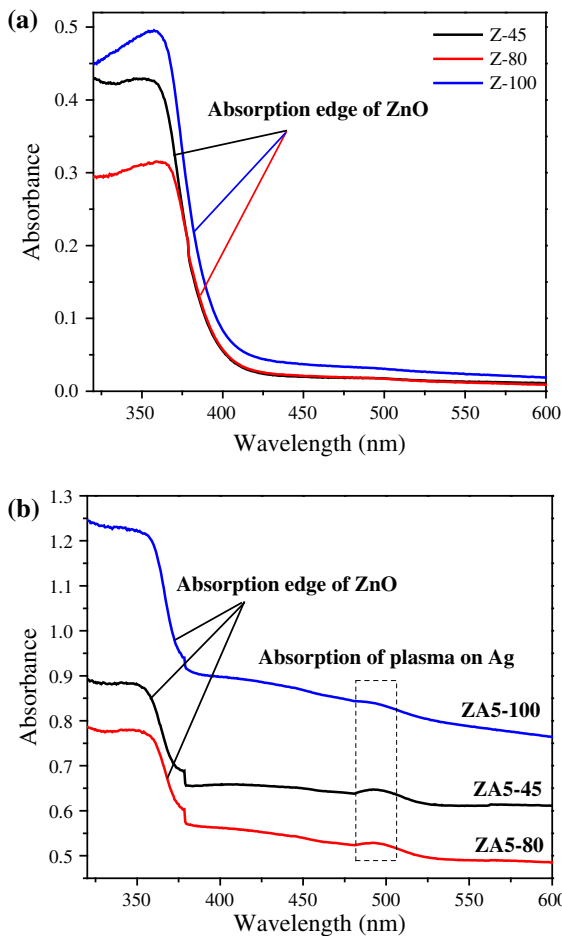


Fig. 5 UV-vis spectra of the catalysts Z-x (a) and ZA5-x (b) even after ultrasonic treatment and electron beam attacking

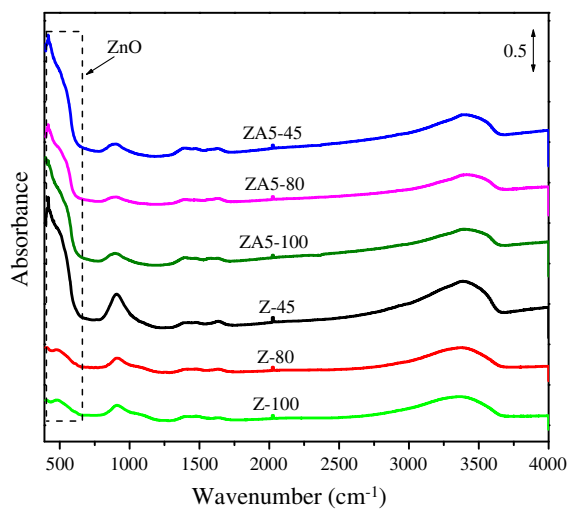


Fig. 6 FT-IR spectra of the catalysts ZA5-x and Z-x

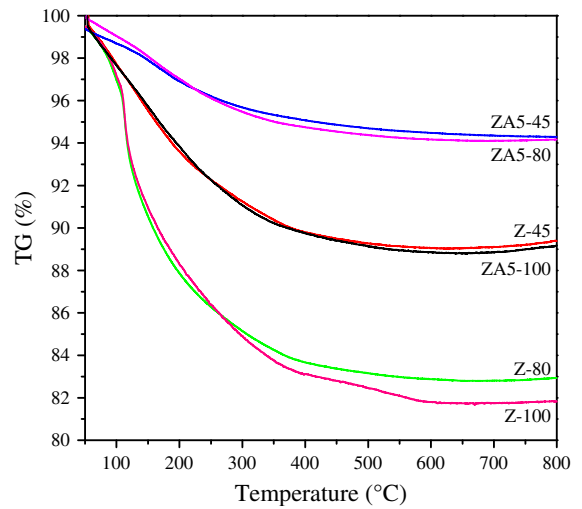


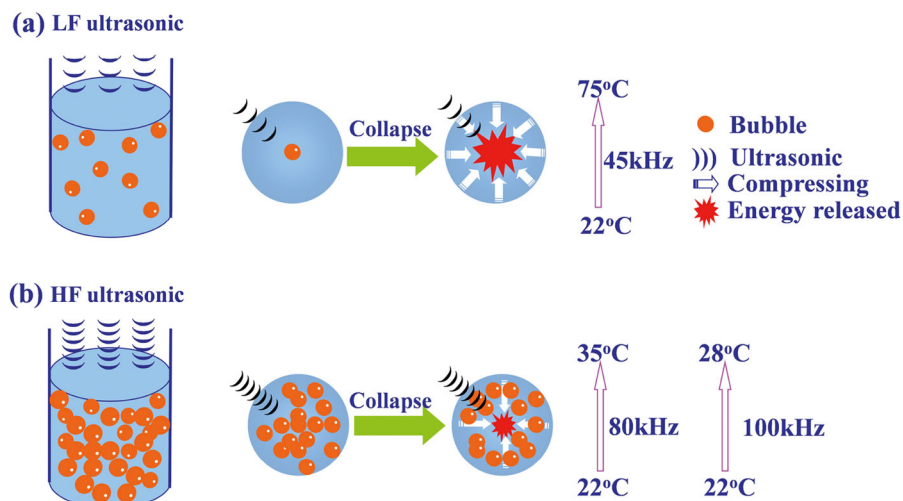
Fig. 7 TG curves of the catalysts ZA5-x and Z-x

Table 1 The weight loss percentage of all the catalysts Z-x and ZA5-x during TG

Catalyst	Weight loss percentage (%)
Z-45	10.5
Z-80	17.0
Z-100	18.0
ZA5-45	6.0
ZA5-80	6.0
ZA5-100	11.0

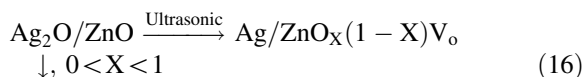
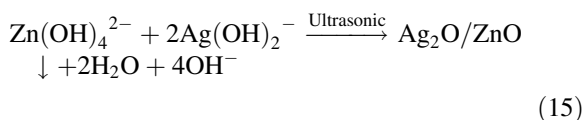
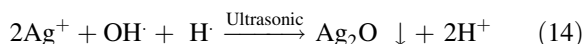
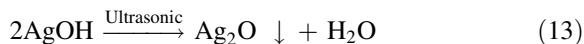
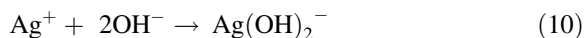
is very high, because the squeezing from the surrounding liquid is very powerful during the adiabatic compression. The hotspots formed here should have very high temperature, which is favorable to the transformation of hydroxide to oxide and the growth of ZnO crystal. However, when high-ultrasonic frequency is used, as shown in Scheme 1b, lots of bubbles can be formed during the ultrasonic irradiation process, and some of them may contact with each other. In this condition, the energy released from the implosive collapse of bubbles should be much less because each bubble is not only surrounded by liquid but also by other bubbles (surrounding bubbles). On one hand, these surrounding bubbles buffer the adiabatic compression process because squeezing is greatly alleviated compared to that when the bubble is only surrounded by liquid; on the other hand, these surrounding bubbles can absorb the energy released

Scheme 1 Energy released from bubble collapse during ultrasonic irradiation: **a** low frequency (LF, 45 kHz); **b** high frequency (HF, 80, and 100 kHz)



from the implosive collapse. Therefore, the temperature of the formed hotspots here is relatively lower, which is apparently unfavorable to the transformation of hydroxide to oxide and the growth of ZnO crystal. In fact, the influence of ultrasonic frequency on the acoustic cavitation effect can also be reflected by the change of temperature during the experiments. As seen from Scheme 1, the temperature of the reaction system corresponding to the ultrasonic frequency of 45, 80, and 100 kHz, increases from 22 to 75, 22 to 35, and 22 to 28 °C, respectively. Therefore, it is confirmed that low-ultrasonic frequency is much better for the formation and growth of ZnO crystal.

After Ag^+ is doped, the following reactions Eqs. 10–16 may also take place besides the Eqs. 1–9. (Bang and Suslick 2010).



The results of TG in Fig. 7 have indicated that the weight loss of ZA5- x is much lower than that of Z- x , which suggests the presence of larger amount of oxides in the catalysts ZA5- x . This phenomenon can be well explained by the reaction between these two kinds of hydroxides as shown in Eq. 15. As a result, all the ZA5- x catalysts show more uniform morphology of ZnO than Z- x catalysts; the scattered irregular blocks and the particles are no longer present in ZA5- x catalysts. Here, it should be mentioned that the effect of Ag^+ on the morphology of ZnO is more obvious when higher ultrasonic frequency is used. For example, Z-100 is mainly composed of irregular blocks, while ZA5-100 mainly consists of some regular flower-like structures.

Photocatalytic activity

Figure 8a shows the photocatalytic activity of ZA5-45 and Z-45 for Rhodamine B photodegradation. For comparison, the blank test was also conducted under the same reaction condition. It can be seen that the rate for Rhodamine B degradation is very low in the absence of catalysts under UV irradiation for 50 min. With the addition of catalysts, the degradation is greatly accelerated, especially for the ZA5-45 which shows much better photocatalytic activity than other catalysts.

Figure 8b shows the linear kinetic fitting plots of $\ln(C_t/C_0) = f(t)$ for Rhodamine B photodegradation over ZA5-45 and Z-45, where C_0 and C_t are the initial concentration of Rhodamine B after the equilibrium adsorption and the reaction concentration of

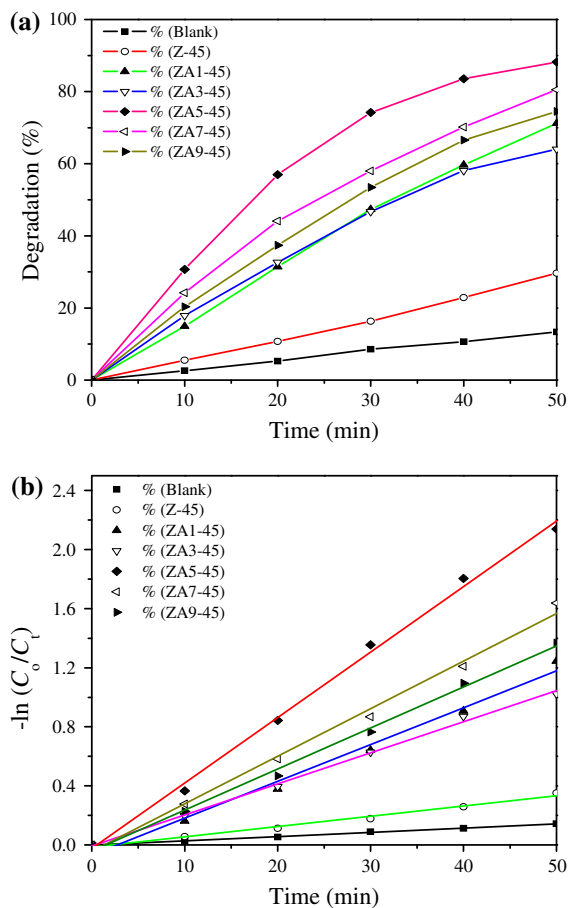


Fig. 8 Activity for Rhodamine B photodegradation (a) and kinetic plots (b) of ZAY-45 and Z-45 catalysts

Rhodamine B at time t , respectively. The linear fitting results are listed in Table 2. It is found that the squares of linear correlation coefficients (R^2) are all larger than 99 %, so the photodegradation of Rhodamine B can be considered as a pseudo-first-order reaction in kinetics, and the slope of the linear $\ln(C_t/C_0) = f(t)$ can be considered as the rate constant k . For comparison, the rate constants for the blank reaction and all the ZAY-45 and Z-45 catalysts are also listed in Table 2. From the rate constant k in Table 2, it can be deduced that the order for the photodegradation rates (r) over the ZAY-45 and Z-45 catalysts is $r(\text{ZA5-45}) > r(\text{ZA7-45}) > r(\text{ZA9-45}) > r(\text{ZA1-45}) > r(\text{ZA3-45}) > r(\text{Z-45})$.

With the same method, the photocatalytic activity and kinetics of Rhodamine B photodegradation over the catalysts prepared using the ultrasonic frequency of 80 kHz (ZAY-80, Z-80) and 100 kHz (ZAY-100,

Z-100) are also studied as shown in Figs. 9 and 10, respectively. The linear kinetic fitting results are also listed in Table 2. The order for the photodegradation rates over ZAY-80 and Z-80 catalysts is $r(\text{ZA5-80}) > r(\text{ZA7-80}) > r(\text{ZA9-80}) > r(\text{ZA1-80}) > r(\text{ZA3-80}) > r(\text{Z-80})$, and that over ZAY-100 and Z-100 catalysts is $r(\text{ZA5-100}) > r(\text{ZA9-100}) > r(\text{ZA7-100}) > r(\text{ZA1-100}) > r(\text{ZA3-100}) > r(\text{Z-100})$. Apparently, the activity of all the ZAY- x catalysts for Rhodamine B photodegradation largely depends on the dosage of Ag; for the three series of the catalysts ZAY-45, ZAY-80, and ZAY-100, the catalysts doped with 5 % Ag always show the highest photodegradation rates. Among the three catalysts with 5 % Ag but using different ultrasonic frequencies in preparation, ZA5-100 exhibits relatively higher photodegradation rate, followed by ZA5-45 and ZA5-80. This difference is probably resulted from the different availabilities of UV light for the samples prepared using different ultrasonic frequencies. Figure 5b has shown that ZA5-100 possesses the highest UV-vis absorbance followed by ZA5-45 and ZA5-80, which is totally consistent with the order of photodegradation rates.

The enhancement effect of Ag on the photocatalytic activity of ZnO is related to the change of Fermi energy levels of Ag and ZnO. It is well known that the Fermi energy level of Ag is higher than that of ZnO. When Ag and ZnO contact, new Fermi energy level (E_f) is formed between the Fermi energy levels of Ag and ZnO so as to achieve a stable state. Therefore, the E_f is still lower than the conduction band of ZnO (Lai et al. 2010). Scheme 2 shows the photocatalytic mechanism on the Ag/ZnO catalyst. After irradiated by the light with energy equal to or higher than the band gap, the electrons in the valence band of ZnO can be excited into the conduction band, leading to the separation of electrons and holes. These excited electrons can be further captured by O_2 to form superoxide radical anion $\cdot\text{O}_2^-$, while the holes can be captured by OH^- to form hydroxide free radical $\cdot\text{OH}$, which are active species for organic dyes photodegradation. To verify this viewpoint, the benzoquinone (BQ) and isopropyl alcohol (IPA) are often adopted as the traps for $\cdot\text{O}_2^-$ and $\cdot\text{OH}$ in photodegradation reaction, respectively (Stylidi et al. 2004; Zhang et al. 2010). As shown in Fig. 11, in this work, the degradation of RhB is also seriously inhibited after addition of BQ or AO in reaction system, which implies that the $\cdot\text{O}_2^-$ and $\cdot\text{OH}$ species should have played major role in the photocatalytic

Table 2 Reaction rate constant (k) and the square of correlation coefficient of kinetic linear fitting for Rhodamine B photodegradation over the catalysts ZAy-x

X	ZAy-45		ZAy-80		ZAy-100	
	k (min ⁻¹)	R^2	k (min ⁻¹)	R^2	k (min ⁻¹)	R^2
Blank	0.0029	0.9990	0.0029	0.9990	0.0029	0.9990
0	0.0070	0.9942	0.0096	0.9901	0.0073	0.9967
1	0.0249	0.9936	0.0236	0.9999	0.0259	0.9996
3	0.0211	0.9986	0.0196	0.9998	0.0238	0.9999
5	0.0443	0.9982	0.0292	0.9995	0.0452	0.9987
7	0.0322	0.9968	0.0286	0.9988	0.0275	0.9994
9	0.0278	0.9979	0.0266	0.9990	0.0310	0.9987

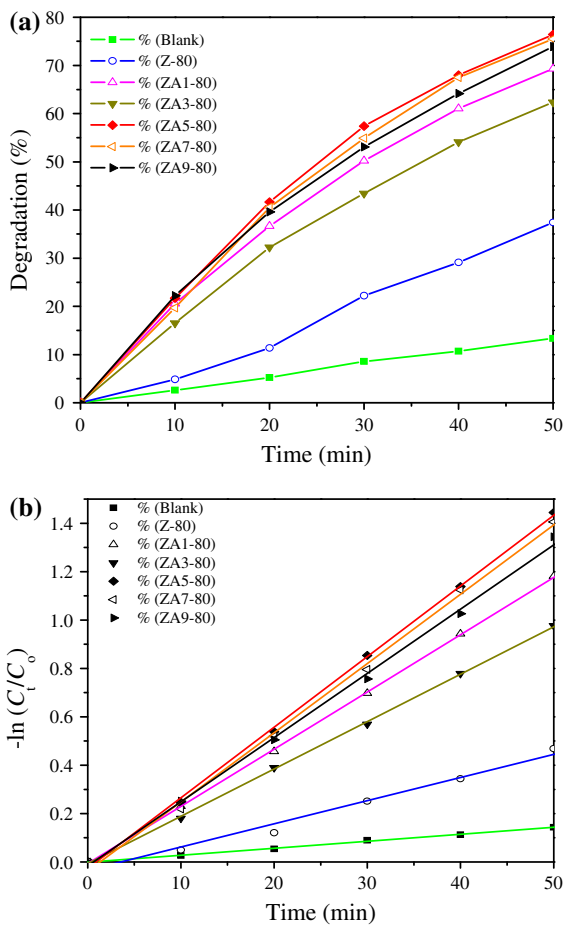


Fig. 9 Activity for Rhodamine B photodegradation (a) and kinetic plots (b) of ZAy-80 and Z-80 catalysts

degradation of RhB. Because of the lower energy level of E_F , the excited electrons in the conduction band of ZnO can flow into Ag which can serve as a sink for excited

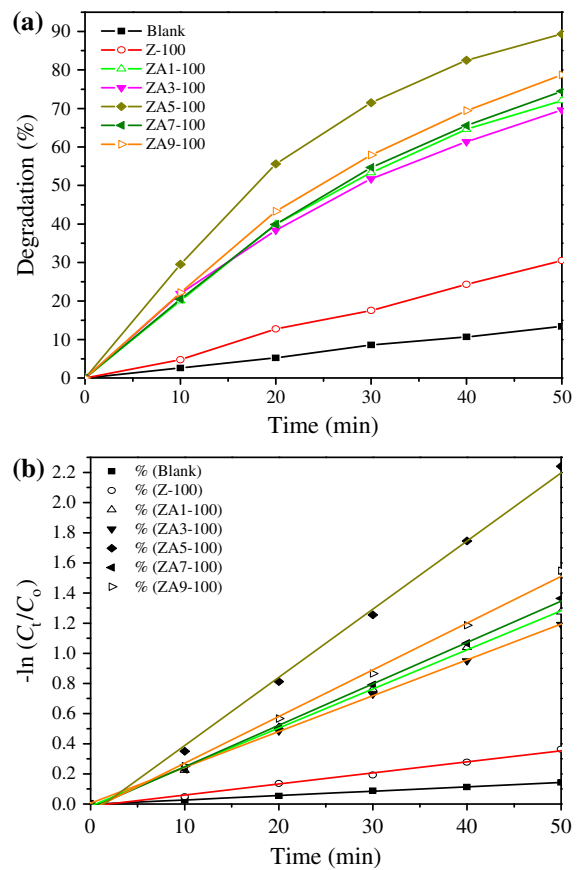
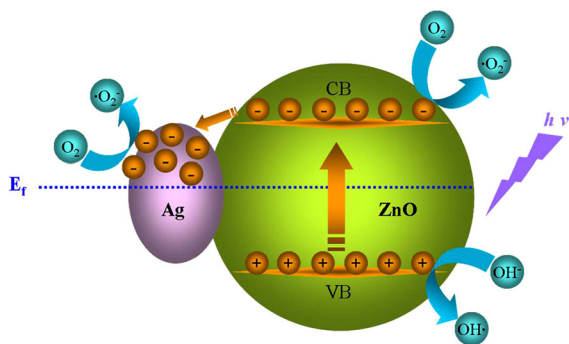


Fig. 10 Activity for Rhodamine B photodegradation (a) and kinetic plots (b) of ZAy-100 and Z-100 catalysts

electrons, thus facilitating the electron–hole segregation. In this condition, the excited electrons not only in the conduction band of ZnO but also in Ag islands can be further captured by O_2 to form superoxide radical anion O_2^- ; as a result, the photocatalytic activity of the



Scheme 2 The photocatalytic mechanism for the Ag/ZnO catalyst

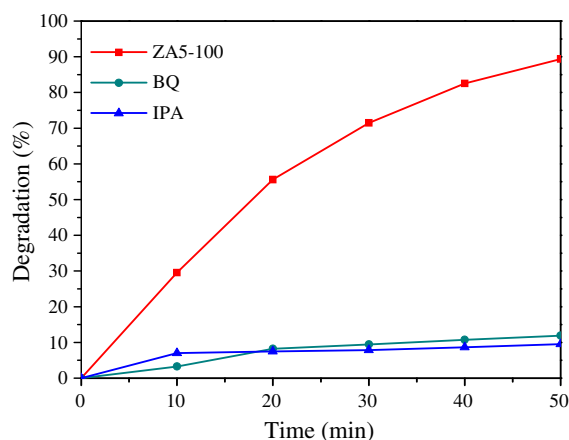


Fig. 11 Activity for Rhodamine B photodegradation over ZA5-100 in the absence & presence of BQ and IPA

catalysts is greatly enhanced (Zheng et al. 2007b; Lai et al. 2010). However, too much Ag may cover the surface of ZnO and block the adsorption of dye, decreasing the availability of UV light and the efficiency of mass transfer.

Conclusion

Flower-like ZnO nano-materials can be successfully prepared by a facile one-step independent ultrasonic irradiation method at ambient condition, and Ag can be readily doped on the surface of ZnO through one-pot reaction. Both the ultrasonic frequency and the doping amount of Ag have great influence on the morphology of ZnO. Low-ultrasonic frequency is much better for the growth of crystal ZnO due to the higher energy released during the acoustic cavitation process. The doping of Ag^+ can promote the

transformation of hydroxide to oxide via the reaction between $\text{Zn}(\text{OH})_4^{2-}$ and $\text{Ag}(\text{OH})_2^-$, thus increasing the yield of ZnO, which is favorable to the formation of flower-like structured ZnO.

The photocatalytic activity of ZnO is remarkably enhanced when Ag is doped. The dispersed Ag can serve as the excited electron sinks, greatly promoting the electron-hole segregation; the optimal doping amount of Ag is 5%; too much Ag is unfavorable to the photocatalytic activity due to the low availability of UV light and the decreased mass transfer efficiency. The ultrasonic frequency used in catalyst preparation also influences the photocatalytic activity. Among the catalysts with optimized amount of Ag (5%), ZA5-100 possesses the highest photocatalytic activity for the degradation of Rhodamine B, which is attributed to its best UV-vis availability.

Experimental section

Catalyst preparation

All the reagents used in this work are in analytical grade without further purification (supplied by Tianjin Guangfu Fine Chemicals Research Institute). All the ZnO catalysts were synthesized by a facile one-step independent ultrasonic irradiation method with frequency modulated. The detailed synthesis procedure is as follows: zinc acetate dihydrate (0.2 g) and citric acid (1.1 g) were first dissolved in distilled water (60 mL) forming a mixed solution, and then another aqueous solution of sodium hydroxide (1 mol L^{-1} , 20 mL) was dropped into this solution under vigorous stirring. The beaker containing above solution was put into an ultrasonic bath (200 W, KQ-200VDE, Kunshan Ultrasonic Instruments Co. Ltd., P. R. China). After ultrasonic irradiation for 1 h at room temperature, the resulting products were centrifuged and washed with water/ethanol in turns for two times to get the solid precursor which was dried at room temperature and used for further characterization. The as-synthesized ZnO catalysts are denoted as Z- x ($x = 45, 80, \text{ and } 100$, respectively, indicating the ultrasonic frequency used in preparation). Another series of Ag/ZnO catalysts were also prepared by the facile one-pot synthesis method, and the preparation procedure is the same as that for Z- x ; the sole difference is the addition of certain amounts of silver nitrate into the mixed

solution of zinc acetate dihydrate and citric acid at the first step. This series of catalysts are denoted as ZAy-x (x represents the ultrasonic frequency; y = 1, 3, 5, 7, and 9 corresponds to the Ag/Zn atomic ratio of 1, 3, 5, 7, and 9 %, respectively).

Catalyst characterization

The X-ray powder diffraction (XRD) was performed on an D/max 2500v/pc (Rigaku) diffraction instrument operating at 200 mA and 40 kV, using Cu K α as radiation source ($\lambda = 0.15418$ nm). The data of 2θ from 20° to 100° were collected with the stepsize of 0.02° .

The surface morphology of the catalysts was determined by using a Hitachi S4800 field-emission scanning electron microscope (SEM). The images of transmission electron microscope (TEM) and high resolution transmission electron microscope (HR-TEM) for the catalysts were obtained using a JEM-2100F system equipped with energy-dispersive X-ray spectrometer (EDS) operating at 200 kV. Before observation, the sample was ultrasonically suspended and deposited on a copper grid.

UV-vis diffuse reflectance spectra (UV-vis DRS) of the catalysts were recorded on a Lambda 750S UV-vis-NIR spectrometer (Perkin-Elmer) equipped with an integrating sphere. The DRS spectra were collected in 200–800 nm against barium sulfate standard.

Fourier transform infrared spectra (FT-IR) were obtained on a Nicolet Nexus spectrometer using KBr as reference. Each time, 1 mg of the powder sample was first mixed with 100 mg KBr, and then the mixture was ground and compressed into tablet for measurement.

Thermogravimetric analysis (TG) was conducted on a Pyris Diamond TG/DTA analyzer (Perkin-Elmer). The samples were heated from room temperature to 800°C at a rate of $10^\circ\text{C min}^{-1}$ in flow air (100 mL min^{-1}).

Evaluation of photocatalytic performance

The photodegradation of Rhodamine B was used as a model reaction to evaluate the photocatalytic activity of the catalysts. Each time, the catalyst (20 mg) was first suspended in aqueous solution of Rhodamine B (1.0×10^{-5} mol L $^{-1}$, 100 mL), then transferred to a beaker, and agitated overnight in dark to achieve equilibrium adsorption. A 250 W high-pressure mercury lamp with a quartz condenser tube around was positioned in the middle of the beaker as UV irradiation

source. Each degradation experiment was continuously conducted for 50 min, and the mixture (3.5 mL) was withdrawn for analysis every 10 min. After separation of the catalyst from the suspension by centrifugation, the after-reacted solution was analyzed by a UV-vis spectrometer (Lambda 750S, Perkin-Elmer) using deionized water as reference (measuring the absorption of Rhodamine B at 554 nm). The degradation efficiency is calculated using the following equation:

$$\begin{aligned} \text{Degradation (\%)} &= (C_0 - C) \times 100 \% / C_0 \\ &= (A_0 - A) \times 100 \% / A_0 \end{aligned}$$

where C_0 and C correspond to the initial and changed concentrations of Rhodamine B during reaction, respectively; and A_0 and A represent the initial and changed absorbance of Rhodamine B at 554 nm, respectively (Lai et al. 2010).

The experiment to verify the $\cdot\text{O}_2^-$ and $\cdot\text{OH}$ as active species is the same as the above process except that BQ (4.3 mM) or IPA (1.0 M) was added into the reaction system, respectively.

Acknowledgments This work is financially supported by the National Natural Science Foundation of China (No.21076146, 21276184, U1332102), the Specialized Research Fund for the Doctoral Program of Higher Education of China (No. 20120032110014), and the Program of New Century Excellent Talents in University of China (No. NCET-07-0599). The authors are also grateful to the Program of Introducing Talents of Discipline to University of China (No. B06006).

References

- Amir O, Aziz H, Mahsa P (2013) Application of ultrasonic irradiation method for preparation of ZnO nanostructures doped with Sb+3 ions as a highly efficient photocatalyst. *Appl Surf Sci* 276:468–475
- Bang JH, Suslick KS (2010) Applications of ultrasound to the synthesis of nanostructured materials. *Adv Mater* 22:1039–1059
- Bhatkhande DS, Pangarkar VG, Beenackers AA (2002) Photocatalytic degradation for environmental applications—a review. *J Chem Technol Biotechnol* 77:102–116
- Buzea C, Pacheco II, Robbie K (2007) Nanomaterials and nanoparticles: sources and toxicity. *Biointerphases* 2: MR17–MR71
- Georgekutty R, Seery MK, Pillai SC (2008) A highly efficient Ag-ZnO photocatalyst: synthesis, properties, and mechanism. *J Phys Chem C* 112:13563–13570
- Gerven TV, Mul G, Moulijn J, Stankiewicz A (2007) A review of intensification of photocatalytic processes. *Chem Eng Process* 46:781–789
- Jung S, Oh E, Lee K, Yang Y, Park C, Park W, Joeng S (2008) Sonochemical preparation of shape-selective ZnO nanostructures. *Cryst Growth Des* 8:265–269

- Klingshirn C, Fallert J, Zhou H, Sartor J, Thiele C, Maier-Flaig F, Schneider D, Kalt H (2010) 65 years of ZnO research – old and very recent results. *Phys Status Solidi B* 247:1424–1447
- Lai Y, Meng M, Yu Y (2010) One-step synthesis, characterizations and mechanistic study of nanosheets-constructed fluffy ZnO and Ag/ZnO spheres used for Rhodamine B photodegradation. *Appl Catal B* 100:491–501
- Lai Y, Meng M, Yu Y, Wang X, Ding T (2011) Photoluminescence and photocatalysis of the flower-like nano-ZnO photocatalysts prepared by a facile hydrothermal method with or without ultrasonic assistance. *Appl Catal B* 105:335–345
- Liu Y, Kang ZH, Chen ZH, Shafiq I, Zapien JA, Bello I, Zhang WJ, Lee ST (2009) Synthesis, characterization, and photocatalytic application of different ZnO nanostructures in array configurations. *Cryst Growth Des* 9:3222–3227
- Liu HR, Shao GX, Zhao JF, Zhang ZX, Zhang Y, Liang J, Liu XG, Jia HS, Xu BS (2012) Worm-like Ag/ZnO core-shell heterostructural composites: fabrication, characterization, and photocatalysis. *J Phys Chem C* 116:16182–16190
- Look DC (2011) Recent advances in ZnO materials and devices. *Mater Sci Eng B* 80:383–387
- Mazloumi M, Zanganeh S, Kajbafvala A, Ghariniyat P, Taghavi S, Lak A, Mohajerani M, Sadrnezhad SK (2009) Ultrasonic induced photoluminescence decay in sonochemically obtained cauliflower-like ZnO nanostructures with surface 1D nanoarrays. *Ultrason Sonochem* 16:11–14
- Mishra P, Yadav RS, Pandey AC (2010) Growth mechanism and photoluminescence property of flower-like ZnO nanostructures synthesized by starch-assisted sonochemical method. *Ultrason Sonochem* 17:560–565
- Murphy CJ, Jana NR (2002) Controlling the aspect ratio of inorganic nanorods and nanowires. *Adv Mater* 14:80–82
- Mccullagh C, Skillen N, Adams M, Robertson PKJ (2011) Photocatalytic reactors for environmental remediation: a review. *J Chem Technol Biotechnol* 86:1002–1017
- Roy S, Basu S (2002) Improved zinc oxide film for gas sensor applications. *Bull Mater Sci* 25:513–515
- Stylidi M, Kondarides D, Verykios X (2004) Visible light-induced photocatalytic degradation of acid orange 7 in aqueous TiO₂ suspensions. *Appl Catal B* 47:189–201
- Suslick KS (1990) Sonochemistry. *Science* 247:1439–1445
- Uma K, Ananthakumar S, Mangalaraja RV, Mahesh KPO, Soga T, Jimbo T (2009) A facile approach to hexagonal ZnO nanorod assembly. *J Sol-Gel Sci Technol* 49:1–5
- Wang ZL (2004) Zinc oxide nanostructures: growth, properties and applications. *J Phys* 16:R829–R858
- Wang ZL, Kong XY, Ding Y, Cao P, Hughes WL, Yang R, Zhang Y (2004) Semiconducting and piezoelectric oxide nanostructures induced by polar surfaces. *Adv Funct Mater* 14:943–956
- Yamamoto Y (2000) Semiconductor physics: half-matter, half-light amplifier. *Nature* 405:629–630
- Zhang Y, Mu J (2007) One-pot synthesis, photoluminescence, and photocatalysis of Ag/ZnO composites. *J Colloid Interface Sci* 309:478–484
- Zhang Q, Chou TP, Russo B, Jenekhe SA, Cao G (2008a) High conversion efficiency in dye-sensitized solar cells through controlled aggregation of ZnO nanocrystallites. *Angew Chem Int Ed* 47:2402–2406
- Zhang J, Zhu P, Li Z, Chen J, Wu Z, Zhang Z (2008b) Fabrication of polycrystalline tubular ZnO via a modified ultrasonically assisted two-step polyol process and characterization of the nanotubes. *Nanotechnology* 19:165605
- Zhang L, Wong K, Yip H, Hu C, Yu J, Chan C, Wong P (2010) Effective photocatalytic disinfection of *E. coli* K-12 using AgBr–Ag–Bi₂WO₆ nanojunction system irradiated by visible light: the role of diffusing hydroxyl radicals. *Environ Sci Technol* 44:1392–1398
- Zhao Q, Xu XY, Song XF, Zhang XZ, Yu DP (2006) Enhanced field emission from ZnO nanorods via thermal annealing in oxygen. *Appl Phys Lett* 88:033102
- Zheng Y, Zheng L, Zhan Y, Lin X, Zheng Q, Wei K (2007a) Ag/ZnO heterostructure nanocrystals: synthesis, characterization, and photocatalysis. *Inorg Chem* 46:6980–6986
- Zheng Y, Chen C, Zhan Y, Lin X, Zheng Q, Wei K, Zhu J, Zhu Y (2007b) Luminescence and photocatalytic activity of ZnO nanocrystals: correlation between structure and property. *Inorg Chem* 46:6675–6682
- Zheng Y, Yu X, Xu X, Jin D, Yue L (2010) Preparation of ZnO particle with novel nut-like morphology by ultrasonic pretreatment and its luminescence property. *Ultrason Sonochem* 17:7–10
- Zhou X, Zhang D, Zhu Y, Shen Y, Guo X, Ding W, Chen Y (2006) Mechanistic investigations of PEG-directed assembly of one-dimensional ZnO nanostructures. *J Phys Chem B* 110:25734–25739